PROCEEDINGS OF SPIE

SPIEDigitalLibrary.org/conference-proceedings-of-spie

Numerical modeling of H-PDLC devices for diffractive optical elements with variable properties

Jorge Francés

Jorge Francés, "Numerical modeling of H-PDLC devices for diffractive optical elements with variable properties," Proc. SPIE 12151, Photosensitive Materials and their Applications II, 1215106 (24 May 2022); doi: 10.1117/12.2627153

SPIE.

Event: SPIE Photonics Europe, 2022, Strasbourg, France

Invited Paper

Numerical modelling of H-PDLC devices for diffractive optical elements with variable properties

Jorge Francés[a,b]

[a]I.U. Física Aplicada a las Ciencias y las Tecnologías, Universidad de Alicante, P.O. Box 99, San Vicente del Raspeig, E-03080, Alicante, Spain
[b]Dpto. Física, Ingeniería de Sistemas y Teoría de la Señal, Universidad de Alicante, P.O. Box 99, San Vicente del Raspeig, E-03080, Alicante, Spain

ABSTRACT

Holographic polymer dispersed liquid crystal devices (H-PDLC) are involved in many applications, e.g. diffraction lenses, optical data storage, and image capture devices. H-PDLC is based on a light-sensitive monomer and liquid crystal (LC) mixture exposed to an interference pattern. The monomer concentration rises in the illuminated area, whereas in the dark zones, the LC is concentrated, setting up LC droplets of fewer nanometers. Accurate knowledge of the elastic behaviour of the LC director distribution and the influence of the boundaries with the polymer matrix can help to optimise the diffraction efficiency or the angular selectivity of these devices, keeping the driving voltage low. Here, a review of the latest analysis for accurately estimating the director distribution in LC-based devices is shown. This analysis is carried on in three steps. Firstly, an accurate model based on creating a considerably high number of droplets surrounding the polymer matrix fringes is performed. In this step, the user can modify the ratio between the areas filled with LC and polymer and the size and aspect ratio of the droplets. This packing step can be very demanding depending on the thickness of the grating and the domain dimensions considered for the analysis (2D or 3D). Secondly, a formulation based on estimating the director distribution is performed to derive the permittivity tensor from the LC director. Thirdly and last, from the information obtained in the previous step, a Finite-Difference Time-Domain simulation is performed to estimate the electromagnetic field distribution inside the domain considered accurately. The diffraction efficiencies and many indirect parameters can be computed from this rigorous analysis.

Keywords: H-PDLC, FDTD, Frank-Oseen Free Energy, Liquid Crystal, LC director

1. INTRODUCTION

The properties of optical and dielectric anisotropy, joint with the non-linear behaviour of LC material to the applied electric field, has become liquid crystals (LC) the focus of many researchers for novel applications [1], i.e. displays, spatial light modulators, tunable lenses; etc. The combination of LC with a high molecular weight polymer matrix sets up what is known as polymer-dispersed liquid crystal (PDLC) devices. In holographic PDLC films, the polymer concentration is high, around 60-70 wt%, the LC droplet size is much smaller than the visible wavelength, and these characteristic forces the application of higher switching voltages. Even the size of the droplets is theoretically small; some LC can have dimensions that induces light scattering. HPDLC alternate polymer-rich and LC-rich regions. This setup is defined by the exposition of the mixture (LC, monomer and photoinitiator (PhI)) with an interference pattern. This interference pattern is produced by the interference of two or multiple coherent laser beams that induce dark (diffusion of LC from bright to dark region) and bright fringes (diffusion of monomer from dart to bright region). These fringes trigger the polymerisation and the phase separation process, thus creating a Bragg grating. The polymer's refractive index is usually chosen to match with the ordinary refractive index of the LC. Hence, HPDLC becomes optically transparent with the application of an electric field. In this case, the LC director is aligned with the field, and there is no grating (OFF state). When the electric field is removed, the orientation of the LC droplets returns to its initial random state, setting up the

Further author information: (Send correspondence to J. Francés)
J. Francés.: E-mail: jfmonllor@ua.es, Telephone: +34 965909951

Photosensitive Materials and their Applications II, edited by Robert R. McLeod, Inmaculada Pascual Villalobos, Yasuo Tomita, John T. Sheridan, Proc. of SPIE Vol. 12151, 1215106 · © 2022 SPIE · 0277-786X · doi: 10.1117/12.2627153

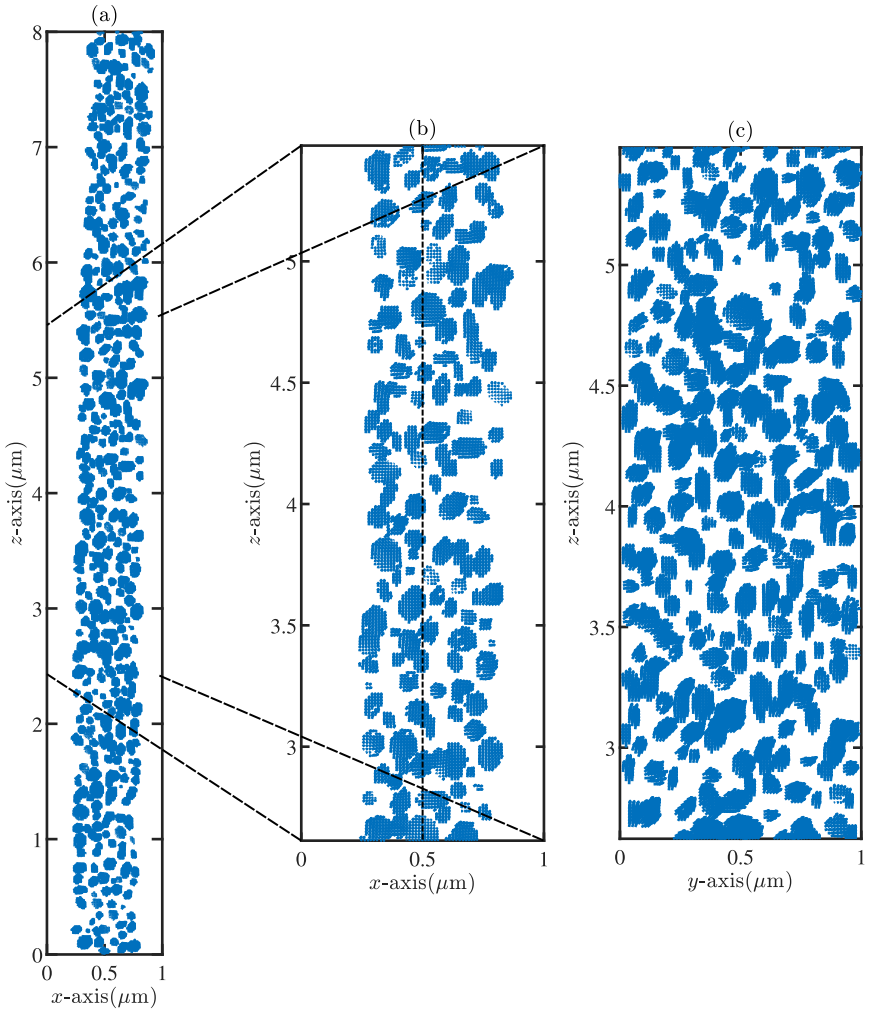

Figure 1. Representation of the initial random LC director through some slices of the H-PDCLC sample generated, here the anchoring strength is W_0=10^{-12} J/m^2 and $\Phi = 0$ V:(**a**) xz plane at $y = 0.5064$ μm. (**b**) Zoom in of a region in the xz plane at $y = 0.5064$ μm. (**c**) Zoom in of a region in the yz plane at $x = 0.5064$ μm. This plane is represented by a vertical dashed line in (**b**).

Bragg grating in ON state. Many researchers have focused their efforts on improving the diffraction efficiency or the angular selectivity with lower driving voltages. To achieve this goal, analytical and numerical approaches have been developed to analyse H-PDLC structures, e. g., the application of Montemezzani's [2] coupled waves theory for gratings to shaped-droplets [3], models of droplet axis reorientation [4], and the effective medium theory [5] applied to the analysis of reflective H-PDLC. It is worth noting the contributions of Kubitskiy *et al.* [6] in the field of numerical analysis through the finite-difference time-domain (FDTD) method of H-PDLC. Regarding the estimation of the LC director inside each LC droplet, it is defined as a unit vector pointing into the (average) direction of the long molecule axis **n** [7]. There are different alternatives for estimating LC director distribution, such as statistically approaches [8] by means of the Monte-Carlo method, or more accurate by minimising the electric and elastic-free energies [7]. In [9] the author considered a two-dimensional split-field (SF) FDTD method for analysing ellipsoidal droplets in H-PDLC gratings with random properties. SF-FDTD is a specified version of the standard FDTD method for analysing electromagnetic waves with an oblique angle of incidence along with periodic media. Readers can find more information about this method in [10, 11, 12]. In [9], the Monte-Carlo method was applied to random ellipsoidal droplets for obtaining the LC director distribution. Many parameters related to the physical packing of the droplets were considered, e.g., the density packing, grating period, upper

and lower limits of the ellipsoid size and initial LC director state. Regarding the random generation of particles and their packing, it is worth mentioning that it is not a straightforward issue. There are many studies that focus on this challenge that affects different disciplines, e.g., biology, engineering [13, 14], and astronomy [15] amongst others. The packing limit for spheres has been well established at a density of $\Omega \approx 0.64$ [14, 16]. However, in this work, lower limits are considered to be closer to non-homogeneous H-PDLC droplets configurations, thus triggering light scattering. In [17] the author extended the work previously mentioned [9] by including a full tensorial three-dimensional numerical analysis carried out using SF-FDTD and estimating the LC director through the minimisation of the total free energy [7, 18]. This process takes into account the contributions of the deformation, surface and electric field [19], i.e., the solution considers the influence of $K_{11}, K_{22}, K_{33}, K_{24}$ elastic constants, anchoring strength, and external field. The influence of the saddle splay constant K_{24} has also been considered since it has a direct influence on the droplet structure, even in the limit of the zero anchoring strength for H-PDLC devices [20, 21] when the surface-to-volume ratio is high [18]. The influence of the K_{13} parameter has been neglected in this work since it has been demonstrated that its anchoring strength at the LC interface is negligible [20].

Fig 1 shows a detail of a sample considered in this work, where a small bending of the interference fringes is shown.

The bending model here considered is the same that the one caused by the pre-stress in photographic emulsions [22]. The LC droplets points are deviated from the standard fringes region using a polynomial of second order.

$$G(z) = W(z)/\Lambda_x = a_0 + a_1 l + a_2 l^2, \tag{1}$$

with $l = z/h$, being h the thickness of the grating and Λ_x the period of the grating. Here $a_0 = a_1 = 0$ and the bending will be mainly produced by the amplitude of a_2. Fig. 2 shows the bending contour lines applied to the position of the LC droplets inside the LC-rich region.

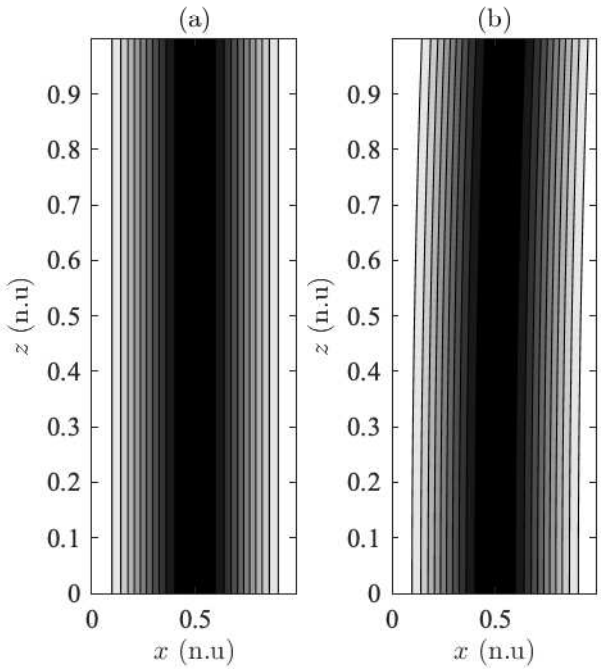

Figure 2. Representation of the bending profile for different parameters of the second. (a) No bending with a_2=0. (b) Bending with $a_2 = 0.3$

2. MODEL

The proposed model is based on a three-dimensional H-PDLC structure that is defined by a finite spatial grid. This mesh is used for solving Maxwell's equations using the SF-FDTD method. Here, light propagates along $\hat{z}$ axis, forming an oblique angle of incidence θ respect of $\hat{x}$ axis. The input light is TE (linear polarisation along y-axis). The incidence plane $\hat{x}\hat{z}$ contains both the wavenumber $\mathbf{k}$ of the input light and the normal to the H-PDLC sample. Periodic boundary conditions (PBC) are applied in both $\hat{y}$ and $\hat{x}$ axis. Perfectly matched layers (PML) are considered at the upper and bottom boundaries in the $\hat{z}$ axis.

The workflow for this numerical analysis is the same that the one shown in [17]. Firstly, the H-PDLC sample is generated through a set of random LC droplets with arbitrary characteristics (considering a set of constraints) and allocated inside the grating following the input parameters provided (period, thickness, LC refractive indices, etc.). Secondly, the estimation of the LC director for each droplet is performed. Each LC droplet is composed of a set of subcells due to the spatial grid considered for the finite-difference scheme. Once the LC orientation is estimated, the permittivity tensor is provided to the SF-FDTD method for computing the light interaction inside the H-PDLC. Interested reader in SF-FDTD formulation can consult some essential references in literature such as [10, 11, 12, 23, 24]. The authors have also contributed in the development of this method in some works [25, 26, 27].

For obtaining the LC director distribution the total free energy is minimised through a relaxation procedure [7, 18, 20] taking into account the influence of the external electric field Φ. Frank elastic free energy density is related to the inhomogenous part of the nematic free energy density as:

$$f_{\mathrm{e}}(\mathbf{r}) = \frac{1}{2}K_{11}(\cdot\mathbf{n})^2 + \frac{1}{2}K_{22}(\mathbf{n}\cdot\nabla\times\mathbf{n})^2 + \frac{1}{2}K_{33}(\mathbf{n}\times\nabla\times\mathbf{n})^2 - \frac{1}{2}K_{24}\nabla\cdot(\mathbf{n}(\nabla\cdot\mathbf{n}) + \mathbf{n}\times\nabla\times\mathbf{n}), \tag{2}$$

where

The interaction of the LC with the surrounding medium can be described as

$$f_{\mathrm{s}}(\mathbf{r}) = (1-(\mathbf{n}\cdot\mathbf{e_r})^2)\frac{W_0}{2}\delta(\mathbf{r}-\mathbf{R}), \tag{3}$$

where $\mathbf{e_r}$ is the preferred anchoring direction on the droplet surface and W_0 the anchoring strength [20]. The vector $\mathbf{R}$ in Eq. (3) represents the points on the droplet surface. Here, the interaction with an external field is described by [7]

$$f_{\mathrm{f}}(\mathbf{r}) = -\frac{1}{2}\boldsymbol{\epsilon}\mathbf{E}\cdot\mathbf{E}, \tag{4}$$

being $\mathbf{E}$ the electric field inside the LC. The dielectric tensor $\boldsymbol{\epsilon}$ of the LC material is related to the director $\mathbf{n}$ by Eq. (3) in [7]. A complete solution of the electric field can be obtained using Maxwell equations while the free energy is minimised. The minimisation of the total free energy is performed by solving the Euler-Lagrange differential equations. This procedure is fully detailed in [7] in Eq. (7), where the electrostatic potential Φ, that is related to the electric field $\mathbf{E}$ through Gauss's law, are iteratively updated.

The packing algorithm creates random LC droplets of size between 25 and 50 nm inside the grating fringes. This size is two times smaller than the results shown in [9]. Users can specify the length of the polymerised area. Here, a grating with the 50% of the period along the x-axis has been considered. Regarding the y-axis, the 100% has been filled with droplets, whereas in [9] this value was 75%. The algorithm identifies the boundaries of the LC droplet and introduces different rotations in order to randomise the sample. The parameters used for the simulations are given in Table 1. LC properties have been extracted from [7] and the value of K_{24} has been considered closer to $K_{11} = K_{22} = K_{33}$ following the results given in [20].

The samples generated have the same thickness d, and, for all samples, a filling factor of the LC droplets inside the polymerised area has been set between 50-51%. The samples have no bending ($a_2 = 0$) or a small bending with a_2=0.15 (see Fig. 1 and Fig. 2). Regarding the SF-FDTD, the wavelength is 633 nm, the spatial resolution has been established by means of a grid density of $N = 25$. Thus the spatial resolution for the SF-FDTD are half the values shown in 1. Regarding the time resolution, it is worth noting that this parameter depends on the Courant stability factor[28], which also is influenced by the angle of incidence. For normal incidence ($\theta_0 = 0°$) $\Delta t \approx s\Delta x/c = 2.11\cdot 10^{-17}$ s. Here, at least 25.000 time-steps have been considered to ensure the steady-state condition of the light inside the H-PDLC structure in all simulations carried on.

Table 1. Parameter values used for numerical simulations.

Parameter description	Symbol	Value
Frank-Oseen elastic coefficients	$K_{11}, K_{22}, K_{33}, K_{24}$	6.82 pN, 3.9 pN, 5.74 pN, 4.00 pN
refractive indices LC	n_e, n_O	1.84, 1.54
refractive index of the polymer	n_{pol}	1.53
relative dielectric permittivity	$\epsilon_{\parallel}, \epsilon_{\perp}$	14, 8.5
thickness of the grating	d	8 μm
cell size	$\Delta x = \Delta y = \Delta z$	12.67 nm
maximum voltage	Φ_{max}	200 V
Wavelength	λ_0	633 nm

3. RESULTS

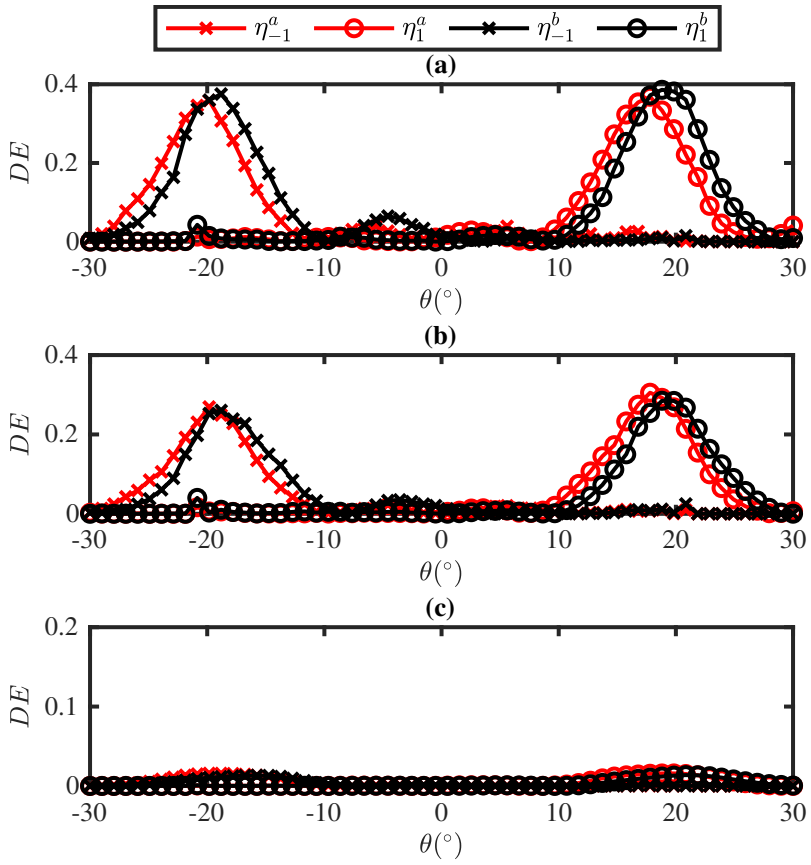

Figure 3. Difraction efficiency of the ±1st-orders as a function of θ (input light incidence angle) for different HPDLC samples (a and b) and different external voltages: (a) Φ=0 V, (b) Φ = 25 V, (c) Φ = 100 V, and (d) Φ = 200 V.

Fig. 3 shows the diffraction efficiency of the ±1st orders as a function of the incidence angle θ (outside the grating) for different voltages and two H-PDLC samples with (upper index b) and without bending (upper index a). The results are solid and demonstrate that the grating tends to vanish as the voltage rises. The results for Φ= 0 V and Φ=75 V almost remain the same, showing that high amplitude voltages are needed to induce an LC director's alignment in the different droplets.

The bending induced on sample b slightly changes the maximum peak position of the diffraction efficiency orders illustrated. The samples' random nature also causes non-symmetries in the curves, demonstrating the

potential of this method to analyse this type of problem from a numerical perspective.

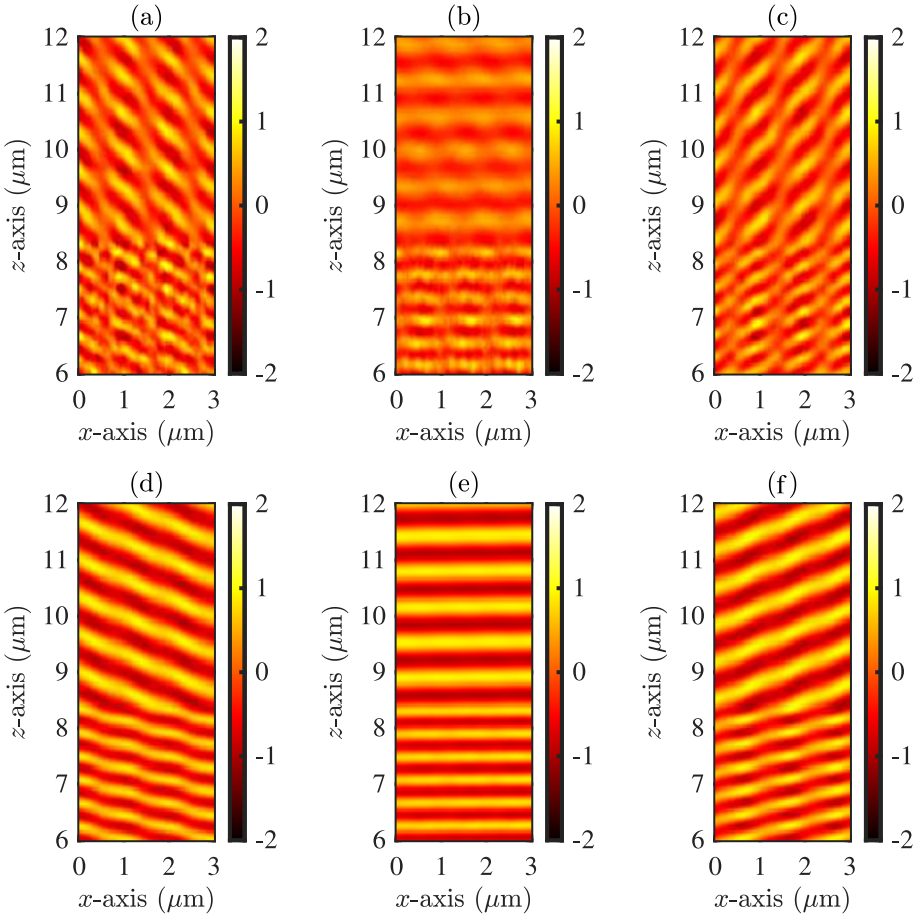

Figure 4. (Video 1) $\Re\{E_y\}$ distribution of the b H-PDLC (with bending) for the xz plane at y=0.5 μm. The units of the field are arbitrary. The ouputu H-PDLC plane is located at z = 8.1 μm. The graphs (a) Φ=0 V and θ_{inc} = -18.8° (b) Φ=0 V and θ_{inc} = 0.5°, (c) Φ=0 V and θ_{inc} = 18.8° (d) Φ=200 V and θ_{inc} = -18.8°, (e) Φ=2000 V and θ_{inc} = 0.5°, (f) Φ=200 V and θ_{inc} = 18.8° (http://dx.doi.org/doi.number.goes.here)

Fig. 4 shows the E_y field component as a function of space for the different samples here considered and different voltages. More precisely, the output plane is represented where interference between 0th- and ±1st-orders can be seen. It is worth noting that considering the setup on Table 1, the maximum efficiency of the ±1st-orders will appear at ±18.34° (Bragg angle defined outside the grating).

Fig. 4(a)-(c) shows the results for the null voltage for the b sample (with bending) and different incidence angles of the input light. For this scenario, the interference between 0th-order and the ±1st-orders can be easily identified in Fig. 4(a) and (c). In Fig. 4(b), close to normal incidence, the ±1st-orders can barely be identified since the 0th-order is more prominent here. In Fig. 4(d)-(f), the same setup is represented but with the maximum external voltage applied. In this situation, the grating presence is minimal, and a small amplitude of the ±1st-orders can be identified in Fig. 4(d) and (f).

4. CONCLUSIONS

In this work, some results related to the analysis of H-PDLC structures using a numerical analysis workflow are shown. More precisely, a set of random H-PDLC samples are created, allocating small LC droplets inside the polymerised region. The LC director distribution is estimated, considering the elastic interactions and the

external voltage applied. The light interaction with the structure is numerically calculated through the SF-FDTD method. All the analyses previously mentioned are carried out in 3D, and the electromagnetic simulation considers a complete tensorial formulation of the electrical permittivity. The size of the droplets has been reduced from previous studies. The morphology of the three-dimensional grating has also been modified by introducing a slight bending along the grating thickness direction. The results have shown similar curves between the H-PDLC samples with and without bending for transmission gratings. The consequences of the bending effect on H-PDLC can barely be identified as a slight curve displacement, and an asymmetry on the lobes of the ±1st diffracted orders. The results show the potential of this scheme that can be applied for characterising H-PDLC samples with a high accuracy taking into account a considerable level of detail of the physical structure.

ACKNOWLEDGMENTS

The work was supported by the "Ministerio de Ciencia e Innovación" of Spain (projects FIS2017-82919-R; PID2019-106601RB-I00), by the "Universidad de Alicante" (UATALENTO18-10;ACIE-20-10), and by Generalitat Valenciana (projects PROMETEO /2021/006, BEST/2021/021; IDIFEDER/2021/014, cofunded by European Union through the FEDER programme).

References

[1] Jain, A. K. and Deshmukh, R. R., "An overview of polymer-dispersed liquid crystals composite films and their applications," in [*Liquid Crystals and Display Technology*], Ghamsari, M. S. and Carlescu, I., eds., ch. 2, IntechOpen, Rijeka (2020).

[2] Montemezzani, G. and Zgonik, M., "Light diffraction at mixed phase and absorption gratings in anisotropic media for arbitrary geometries," *Phys. Rev. E* **55**, 1035–1047 (Jan 1997).

[3] Sutherland, R. L., "Polarization and switching properties of holographic polymer-dispersed liquid-crystal gratings. i. theoretical model," *J. Opt. Soc. Am. B* **19**, 2995–3003 (Dec 2002).

[4] Wu, B.-G., Erdmann, J. H., and Doane, J. W., "Response times and voltages for pdlc light shutters," *Liquid Crystals* **5**(5), 1453–1465 (1989).

[5] Sutherland, R. L., Tondiglia, V. P., Natarajan, L. V., Lloyd, P. F., and Bunning, T. J., "Coherent diffraction and random scattering in thiol-ene–based holographic polymer-dispersed liquid crystal reflection gratings," *Journal of Applied Physics* **99**(12), 123104 (2006).

[6] Kubitskiy, V., Reshetnyak, V., and Galstian, T., "Electric Field Control of Diffraction Efficiency in Holographic Polymer Dispersed Liquid Crystal," *Molecular Crystals and Liquid Crystals* **438**(1), 283/[1847]–290/[1854] (2005).

[7] Moser, S., Ritsch-Marte, M., and Thalhammer, G., "Model-based compensation of pixel crosstalk in liquid crystal spatial light modulators," *Optics Express* **27**(18), 25046 (2019).

[8] Kubytskyi, V. and Reshetnyak, V., "Finite-difference time-domain method calculation of light propagation through H-PDLC," *Semiconductor Physics, Quantum Electronics & Optoelectronics* **10**(1), 83–87 (2007).

[9] Bleda, S., Francés, J., Gallego, S., Márquez, A., Neipp, C., Pascual, I., and Beléndez, A., "Numerical analysis of h-pdlc using the split-field finite-difference time-domain method," *Polymers* **10**(5) (2018).

[10] Oh, C. and Escuti, M. J., "Time-domain analysis of periodic anisotropic media at oblique incidence: an efficient FDTD implementation.," *Optics express* **14**, 11870–84 (nov 2006).

[11] Oh, C. and Escuti, M. J., "Numerical analysis of polarization gratings using the finite-difference time-domain method," *Physical Review A* **76**(4), 043815 (2007).

[12] Miskiewicz, M. N., Bowen, P. T., and Escuti, M. J., "Efficient 3D FDTD analysis of arbitrary birefringent and dichroic media with obliquely incident sources," *Proc. of SPIE* **8255**, 82550W–82550W–10 (feb 2012).

[13] Aste, T. and Weaire, D., [*The Pursuito of Perfect Packing*], Taylor & Francis, Boca Raton, Fla., 2 ed.

[14] Delaney, G. W. and Cleary, P. W., "The packing properties of superellipsoids," *EPL (Europhysics Letters)* **89**, 34002 (feb 2010).

[15] Bagatin, A. C. and Petit, J. M., "Effects of the Geometric Constraints on the Size Distributions of Debris in Asteroidal Fragmentation," *Icarus* **149**(1), 210–221 (2001).

[16] BERNAL, J. D. and MASON, J., "Packing of Spheres: Co-ordination of Randomly Packed Spheres," *Nature* **188**(4754), 910–911 (1960).

[17] Francés, J., Bleda, S., Puerto, D., Gallego, S., Márquez, A., Neipp, C., Pascual, I., and Beléndez, A., "Accurate, efficient and rigorous numerical analysis of 3d h-pdlc gratings," *Materials* **13**(17) (2020).

[18] Yang, D. K. and Wu, S. T., [*Fundamentals of Liquid Crystal Devices*] (2015).

[19] Abdulhalim, I. and Menashe, D., "Approximate analytic solutions for the director profile of homogeneously aligned nematic liquid crystals," *Liquid Crystals* **37**(2), 233–239 (2010).

[20] Žumer, S. and Kralj, S., "Influence of k24 on the structure of nematic liquid crystal droplets," *Liquid Crystals* **12**(4), 613–624 (1992).

[21] Kralj, S. and Žumer, S., "Fréedericksz transitions in supra-m nematic droplets," *Physical Review A* **45**(4), 2461–2470 (1992).

[22] Kubota, T., "The bending of interference fringes inside a hologram," *Optica Acta: International Journal of Optics* **26**(6), 731–743 (1979).

[23] Roden, J., Gedney, S., Kesler, M., Maloney, J., and Harms, P., "Time-domain analysis of periodic structures at oblique incidence: orthogonal and nonorthogonal FDTD implementations," *IEEE Transactions on Microwave Theory and Techniques* **46**, 420–427 (apr 1998).

[24] Shahmansouri, A. and Rashidian, B., "Comprehensive three-dimensional split-field finite-difference time-domain method for analysis of periodic plasmonic nanostructures: near- and far-field formulation," *JOSA B* **28**, 2690 (oct 2011).

[25] Francés, J., Bleda, S., Neipp, C., Márquez, A., Pascual, I., and Beléndez, A., "Performance analysis of the {FDTD} method applied to holographic volume gratings: Multi-core {CPU} versus {GPU} computing," *Computer Physics Communications* **184**(3), 469 – 479 (2013).

[26] Francés, J., Bleda, S., Álvarez, M. L., Martínez, F. J., Márquez, A., Neipp, C., and Beléndez, A., "Acceleration of split-field finite difference time-domain method for anisotropic media by means of graphics processing unit computing," *Optical Engineering* **53**(1), 011005–011005 (2013).

[27] Francés, J., Tervo, J., and Neipp, C., "Split-field finite-difference time-domain scheme for Kerr-type nonlinear periodic media," **134**, 559–579 (2013).

[28] Taflove, A. and Hagness, S. C., [*Computational electrodynamics: The finite-difference time-domain method*], Artech House, third ed. (2005).